STATUS OF EXCLUSION LIMITS OF THE KK-PARITY NON-CONSERVING RESONANCE PRODUCTION WITH UPDATED 13 TeV LHC*

Avirup Shaw

Department of Theoretical Physics
Indian Association for the Cultivation of Science
2A & 2B Raja S.C. Mullick Road, Jadavpur, Kolkata 700 032, India
avirup.cu@gmail.com

(Received February 2, 2018; accepted May 16, 2018)

Unequal strengths of boundary localised terms lead to non-conservation of the Kaluza–Klein (KK) parity in the 4+1 Universal Extra Dimensional model. Consequently, the first excited KK-partners of Standard Model particles are not stable by any symmetry. In this article, using the latest 13 TeV Large Hadron Collider (LHC) results, we revisit the resonant production of first KK-excitations of the neutral gauge bosons (G^1, B^1 and W_3^1) and their subsequent decay. Specifically, G^1 (first KK-excitation of gluon) decays to $t\bar{t}$ pair and B^1/W_3^1 (first KK-excitation of electroweak gauge bosons) decay to $\ell^+\ell^-(\ell \equiv e, \mu)$ pair. We find that the exclusion limits of model parameters obtained at 95% C.L. from the non-observation of these channels have been shifted towards the lower side of the parameter space compared to our previous analysis at 8 TeV.

DOI:10.5506/APhysPolB.49.1421

1. Introduction

After a long anticipation, LHC at Run 1 has been able to discover only the missing piece of the Standard Model (SM) called Higgs boson [1, 2]. At the same time, it is unable to resolve any puzzle among the different long-standing issues (dark matter, neutrino mass and mixing, gauge hierarchy, CP violation, *etc.*) of SM. Even any new physics beyond SM (BSM) has not been detected. In the present days, the LHC is now running at $\sqrt{S} = 13$ TeV. The prime goal of Run 2 is to look for BSM signature. However, both the collaborations ATLAS and CMS have only reported some small local excesses [3, 4] over the SM predictions, which need to be verified by thorough analysis at Run 2. At this moment, it would be a very relevant job to study or revisit

* Funded by SCOAP[3] under Creative Commons License, CC-BY 4.0.

the exclusion limits of the existing BSM physics. In the literature, we have found several examples where the various collaborating groups have updated their existing results with new data. For example, in the context of minimal supersymmetric Standard Model (MSSM), there are two references [5, 6] where Bhattacherjee *et al.* have studied the status of 98 GeV Higgs boson with different versions of the LHC data. With this spirit in Universal Extra Dimensional (UED) model, one of the popular incarnations of BSM physics, we re-examine the exclusion limits achieved via non-observation of resonance production driven by KK-parity non-conserving interactions in the light of 13 TeV LHC data [7, 8].

The UED model [9] is characterised by an extra space-like dimension y which is flat and compactified on a circle S^1 of radius R. All the SM particles can access the dimension y. From the four-dimensional (4-D) point of view, each of the SM particles has infinite towers of KK-modes specified by an integer n, called the KK-number. $n = 0$ modes are labelled as the SM particles. KK-number of a particle is a measure of its momentum along the fifth direction (y). One might expect KK-number to be a conserved quantity by the virtue of extra dimensional momentum conservation. However, a Z_2 symmetry ($y \to -y$) has been imposed to incorporate SM chiral fermions. Consequently, the translational symmetry along the extra dimension is destroyed and we encounter KK-number non-conserving interactions. The compactified space is now called S^1/Z_2 orbifold which extends only from $y = 0$ to $y = \pi R$. After orbifolding, however, a subgroup of KK-number conservation known as KK-parity[1] can still remain a symmetry of 4-D action. KK-parity of a state (labelled with KK-number n) is defined as $(-1)^n$. This parity ensures the stability of lightest ($n = 1$) KK-particle (LKP) which can be treated as a potential dark matter candidate in this scenario. Phenomenology of this UED model from the different perspective can be found in the literature [10–26].

The effective mass profile of a particle at n^{th} KK-level is $\sqrt{m^2+(nR^{-1})^2}$, m being the corresponding SM mass which is very much lower than R^{-1}. Therefore, this model suffers from a deficiency due to the degenerate mass spectrum. Nevertheless, this mass degeneracy could be avoided by radiative corrections. There are two types of radiative corrections, one is called finite bulk correction, while the other is called boundary correction depending on logarithmic value of cut-off[2] scale Λ. Thus it will be relevant to incorporate 4-D kinetic, mass and other necessary interaction terms for the KK-states at the two special points ($y = 0$ and $y = \pi R$) of S^1/Z_2 orbifold. Because these

[1] This KK-parity is equivalent to reflection symmetry of the action with respect to the line $y = \frac{\pi R}{2}$.

[2] UED is an extra dimensional theory and hence should be treated as an effective theory valid up to cut-off scale Λ.

terms can be treated as necessary counterterms for cut-off-dependent loop-induced contributions [27–29] of the five-dimensional (5-D) theory. A very special assumption has been taken in the minimal UED (mUED) models such that the loop-induced contributions exactly vanish at the cut-off scale Λ. However, this unique simplification can be discarded. Even without performing the actual radiative corrections, one might consider kinetic, mass as well as other interaction terms localised at the fixed boundary points ($y = 0$ and $y = \pi R$) to parametrise these unknown corrections. Hence this scenario is known as non-minimal UED (nmUED) [30–36]. Coefficients of different boundary localised terms (BLTs) as well as the radius of compactification (R) can be identified as free parameters of this model. One can constrain these parameters using several experimental inputs. In literature, one finds the bounds on the values of BLT parameters from the consideration of electroweak observables [35], S, T and U parameters [33, 37, 38], relic abundance [39, 40], SM Higgs boson production and its decay [41], study of the LHC experiments [42–44], R_b [45], branching fraction of $B_s \to \mu^+\mu^-$ [38] and $B \to X_s\gamma$ [46], flavour-violating rare top decay [47], $\mathcal{R}(D^{(*)})$ [48] and unitarity of scattering amplitudes involving KK-excitations [49].

In this article, we create non-conservation of KK-parity[3] by adding boundary localised terms of unequal strengths [36, 43, 44]. Consequently, $n = 1$ KK-states are no longer stable and decay to pair of SM particles. Capitalising on this KK-parity non-conserving coupling, we revisit the resonant production of KK-excitations of the neutral gauge bosons at the LHC and their subsequent decay into the SM fermion pair. We use the latest LHC data of CMS [7] and ATLAS [8] collaborations for search of resonant high-mass new phenomena in top–antitop quark pairs ($t\bar{t}$) and dilepton ($\ell^+\ell^-$) final states respectively. From this analysis, we will put constraints on the BLT parameters as well as on the size of the radius of compactification.

The plan of this article is as follows. First, we discuss the relevant couplings and masses in the framework of UED with unequal strength of BLT parameters. We then revisit the exclusion limits obtained via $t\bar{t}$ signal from G^1 production and $\ell^+\ell^-$ signal from the combined production of the B^1 and W_3^1 at the 13 TeV LHC. Furthermore, we compare the limits obtained from the current analysis with those from our previous 8 TeV analyses [43, 44]. Subsequently, we will explore the reasons for which we will obtain the deviation of the limits (in each case for both signal) at 13 TeV LHC. Finally, we will summarise the results.

[3] This can be viewed as R-parity non-conservation in supersymmetry.

2. A glimpse of KK-parity-non-conserving nmUED

In this section, we discuss the primitive terminologies of KK-parity non-conserving nmUED [36, 43, 44]. For the purpose of detailed analysis of the model, we refer to [30–36]. In the following action, we choose the unequal strengths of the boundary terms at the two boundary points ($y = 0$ and $y = \pi R$). Consequently, the KK-parity will not be conserved anymore. However, if the strengths of the boundary terms be equal, then the KK-parity will be restored and we can have the potential dark matter candidate [40].

Let us begin with the action of 5-D fermionic fields $\Psi_{\rm L,R}$ including boundary localised kinetic terms (BLKTs) [34, 36, 43, 44]

$$S_{\rm fermion} = \int {\rm d}^5x \left[\bar{\Psi}_{\rm L} i\Gamma^M D_M \Psi_{\rm L} + \left\{r_f^a \delta(y) + r_f^b \delta(y-\pi R)\right\} \bar{\Psi}_{\rm L} i\gamma^\mu D_\mu P_{\rm L} \Psi_{\rm L} \right.$$
$$\left. + \bar{\Psi}_{\rm R} i\Gamma^M D_M \Psi_{\rm R} + \left\{r_f^a \delta(y) + r_f^b \delta(y-\pi R)\right\} \bar{\Psi}_{\rm R} i\gamma^\mu D_\mu P_{\rm R} \Psi_{\rm R}\right] , \quad (1)$$

where $M = (0, 1 \ldots 4)$ and r_f^a, r_f^b are the coefficients[4] of the BLKTs localised at the two fixed points ($y = 0$ and $y = \pi R$). We can decompose the 5-D four-component fermion fields $\Psi_{\rm L,R}$ into two-component chiral spinors using the following relations [34, 36, 43, 44]:

$$\Psi_{\rm L}(x,y) = \begin{pmatrix} \phi_{\rm L}(x,y) \\ \chi_{\rm L}(x,y) \end{pmatrix} = \sum_n \begin{pmatrix} \phi_{\rm L}^{(n)}(x) f_{\rm L}^n(y) \\ \chi_{\rm L}^{(n)}(x) g_{\rm L}^n(y) \end{pmatrix} , \quad (2)$$

$$\Psi_{\rm R}(x,y) = \begin{pmatrix} \phi_{\rm R}(x,y) \\ \chi_{\rm R}(x,y) \end{pmatrix} = \sum_n \begin{pmatrix} \phi_{\rm R}^{(n)}(x) f_{\rm R}^n(y) \\ \chi_{\rm R}^{(n)}(x) g_{\rm R}^n(y) \end{pmatrix} . \quad (3)$$

Applying suitable boundary conditions [31, 36], we can have the following KK-wave-functions which are simply denoted by f for illustrative purposes [31, 36, 43, 44]:

$$f^n(y) = N_n \left[\cos(m_n y) - \frac{r_f^a m_n}{2} \sin(m_n y)\right] , \qquad 0 \le y < \pi R ,$$
$$f^n(y) = N_n \left[\cos(m_n y) + \frac{r_f^a m_n}{2} \sin(m_n y)\right] , \qquad -\pi R \le y < 0 . \quad (4)$$

KK-masses m_n for $n = 0, 1, \ldots$ satisfy the following transcendental equation [31, 36, 43, 44]:

$$\left(r_f^a r_f^b \; m_n^2 - 4\right) \tan(m_n \pi R) = 2 \left(r_f^a + r_f^b\right) m_n . \quad (5)$$

[4] To respect the chiral symmetry, we have chosen equal strengths of BLKTs for both fermion fields $\Psi_{\rm L,R}$.

For the purpose of illustration, we have chosen two different strategies to study the KK-parity non-conservation. In the first case, we demand that the strength of BLKTs (at two fixed points $y = 0$ and $y = \pi R$) is equal for fermions, *i.e.*, $r_f^a = r_f^b \equiv r_f$, while for the second case, BLKTs vanish at one of the fixed boundary points. For the latter case, we choose $r_f^a \neq 0$, $r_f^b = 0$ and, in this situation, Eq. (5) reduces to [31, 36, 43, 44]

$$\tan(m_n \pi R) = -\frac{r_f^a m_n}{2} \,. \tag{6}$$

N_n is the normalisation constant for n^{th} KK-mode and obtained from orthonormality condition [31, 36, 43, 44]

$$\int_0^{\pi R} \mathrm{d}y \left[1 + r_f^a \delta(y) + r_f^b \delta(y - \pi R)\right] f^n(y)\ f^m(y) = \delta^{nm} \,. \tag{7}$$

For the first case,

$$N_n = \sqrt{\frac{2}{\pi R}} \left[\frac{1}{\sqrt{1 + \frac{r_f^2 m_n^2}{4} + \frac{r_f}{\pi R}}}\right] , \tag{8}$$

when strength of boundary terms is equal *i.e.*, $r_f^b = r_f^a \equiv r_f$. And for the second situation when $r_f^b = 0$ and we set $r_f^a \equiv r_f$, one finds

$$N_n = \sqrt{\frac{2}{\pi R}} \left[\frac{1}{\sqrt{1 + \frac{r_f^2 m_n^2}{4} + \frac{r_f}{2\pi R}}}\right] . \tag{9}$$

To this end, let us discuss the values of BLT parameters which we would like to use in our analysis. If $\frac{r_f^a}{R}$ ($\ll 1$), the KK-mass formula approximately reduces to (using Eq. (6)) [44]

$$m_n \approx \frac{n}{R}\left(\frac{1}{1 + \frac{r_f^a}{2\pi R}}\right) \approx \frac{n}{R}\left(1 - \frac{r_f^a}{2\pi R}\right) . \tag{10}$$

It is evident from the above expression that the KK-mass reduces with increasing positive values of r_f^a. This feature also holds good when the BLKTs are non-vanishing at both the boundary points.

Now, it is clear from Eqs. (8) and (9) that for $\frac{r_f}{R} < -\pi$ (when BLKTs are present at the two boundary points) and $\frac{r_f}{R} < -2\pi$ (when BLKTs are present only at one of the two boundary points), the squared norm of zero mode solutions becomes negative. Furthermore, for $\frac{r_f}{R} = -\pi$ (when BLKTs are present at the two boundary points) and $\frac{r_f}{R} = -2\pi$ (when BLKTs are present only at one of the two boundary points), the solutions turn out to be divergent. Beyond these limits, the fields behave like ghost fields and, consequently, the values of $\frac{r_f}{R}$ beyond these region should be discarded. Moreover, analysis of electroweak precision data reveals that the negative values of BLT parameters are not so competitive [38]. Furthermore, negative values of BLT parameters are less attractive due to phase-space consideration as negative values of BLT parameters enhance the KK-mass which, in turn, suppresses the production cross section. Hence, we will use the positive values of BLKTs in the rest of our analysis.

Let us turn to the action for the 5-D gauge fields. In the presence of BLKTs at the boundary points ($y = 0$ and $y = \pi R$), this can be written down as [36, 43, 44]

$$\begin{aligned} S_V \;=\; -\frac{1}{4}\int \mathrm{d}^5x \Big[& G^{\lambda}_{MN}G^{\lambda MN} + \Big\{ r^a_G\delta(y) + r^b_G\delta(y-\pi R)\Big\} G^{\lambda}_{\mu\nu}G^{\lambda\mu\nu} \\ & + W^i_{MN}W^{iMN} + \Big\{ r^a_W\delta(y) + r^b_W\delta(y-\pi R)\Big\} W^i_{\mu\nu}W^{i\mu\nu} \\ & + B_{MN}B^{MN} + \Big\{ r^a_B\delta(y) + r^b_B\delta(y-\pi R)\Big\} B_{\mu\nu}B^{\mu\nu}\Big] \,. \end{aligned} \tag{11}$$

Here, r^a_V and r^b_V ($V \equiv G, W, B$) parametrise the strength of the BLKTs for the gauge fields. 5-D field strength tensors are given below

$$\begin{aligned} G^{\lambda}_{MN} &\equiv \left(\partial_M G^{\lambda}_N - \partial_N G^{\lambda}_M - \tilde{g}_3 f^{\lambda\rho\sigma} G^{\rho}_M G^{\sigma}_N\right) , \\ W^i_{MN} &\equiv \left(\partial_M W^i_N - \partial_N W^i_M - \tilde{g}_2 \epsilon^{ijk} W^j_M W^k_N\right) , \\ B_{MN} &\equiv \left(\partial_M B_N - \partial_N B_M\right) . \end{aligned} \tag{12}$$

G^{λ}_M ($\lambda = 1, \ldots 8$), W^i_M ($i = 1, 2, 3$) and B_M are the 5-D gauge fields corresponding to $\mathrm{SU}(3)_C$, $\mathrm{SU}(2)_\mathrm{L}$ and $\mathrm{U}(1)_Y$ gauge group respectively. Generically y-dependent KK-wave-functions for the gauge fields ($V_M \equiv (V_\mu, V_4)$) can be written in the following way [36, 43, 44]:

$$V_\mu(x,y) = \sum_n V^{(n)}_\mu(x) a^n(y)\,; \qquad V_4(x,y) = \sum_n V^{(n)}_4(x) b^n(y)\,. \tag{13}$$

A convenient gauge choice[5] for this model would be putting $V_4 \to 0$. This gauge choice would easily eliminate the undesirable terms in which V_μ

[5] A general analysis on gauge-fixing action and gauge-fixing mechanism in the nmUED model can be found in [50].

couples to V_4 via derivative [36, 43, 44]. This is the main purpose of gauge-fixing mechanism. As we are interested in V_μ and its interactions with other physical particles, setting $V_4 \to 0$ is as good as unitary gauge [36, 43, 44].

KK-masses for gauge fields are very similar to the fermions and can be obtained from Eqs. (5) and (6) in a similar manner. The detailed discussions on the gauge fields in nmUED model is readily available in [36].

Furthermore, in Ref. [50], we have shown that when the gauge symmetry is spontaneously broken, the BLKT parameters of gauge bosons and Higgs should be equal for the purpose of proper gauge-fixing. This condition leads to the equality of BLKT parameters of $\mathrm{SU(2)_L}$ and $\mathrm{U(1)}_Y$ gauge bosons *i.e.*, $(r_B^a = r_W^a \equiv r_V^a)$ and $(r_B^b = r_W^b \equiv r_V^b)$. Hence, KK-masses of B and W_3 are equal. However, for the $\mathrm{SU(3)}_C$ gauge boson, we can independently choose the BLKT parameters (r_G^a, r_G^b), which are different from the electroweak sector.

In the different panels ((a), (b), (c) and (d)) of Fig. 1, we have plotted dependence of scaled KK-mass for the first KK-excited gauge fields $G(\equiv$ gluon) and $V(\equiv W_3, B)$ with respect to appropriate ranges of BLKT

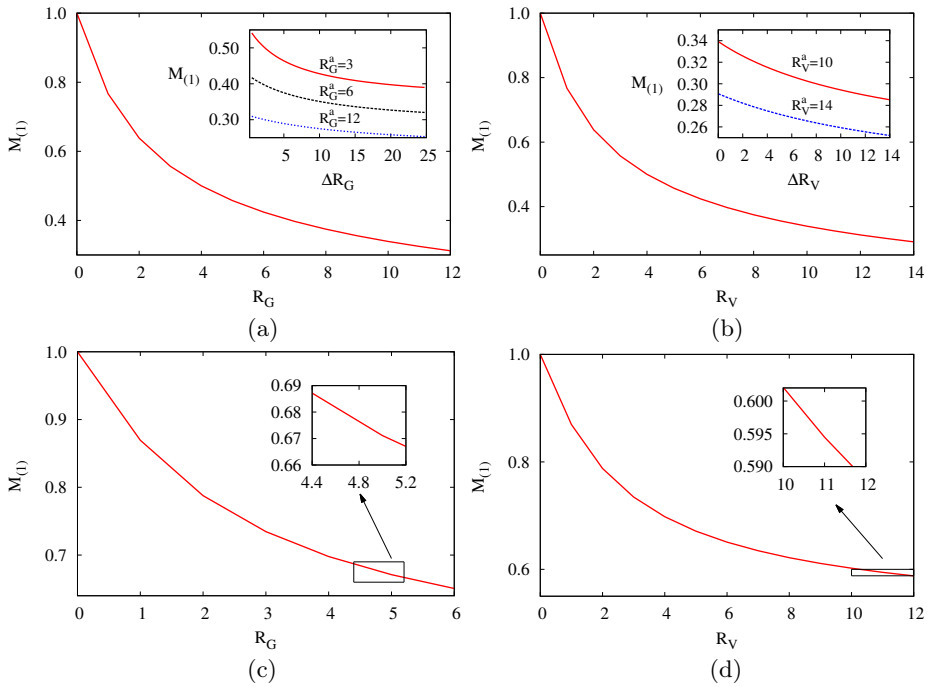

Fig. 1. Left side: The upper (a) and lower (c) panels show the variation of $M_{(1)}(= m_{G^{(1)}}R)$ as a function of BLKT parameters which we will use in $t\bar{t}$ production. Similarly, the upper (b) and lower (d) panels of the right-hand side show the variation of $M_{(1)}(= m_{V^{(1)}}R)$ corresponding to $\ell^+\ell^-$ production. For the purpose of detailed illustrations, one can see the text and also Refs. [36, 43, 44].

parameters what we use in our main analysis. However, the characteristics are similar for all kind of fields. In the upper panels ((a) and (b)), we have shown the mass profile with respect to $R_\alpha(= r_\alpha R^{-1})$ in the symmetric limit $(R^a_\alpha = R^b_\alpha \equiv R_\alpha)$ $(\alpha \equiv G, B, W_3)$. In the inset, we have presented the variation of $M_{(1)}(= m_{\alpha^{(1)}} R)$ with asymmetric parameter $\Delta R_\alpha(= (r^b_\alpha - r^a_\alpha)R^{-1})$, for different choices of R^a_α. Similarly, in the lower panels ((c) and (d)), we have presented the variation of $M_{(1)}$ with respect to $R_\alpha(= r_\alpha R^{-1})$ when boundary terms are present only at the boundary point $y = 0$. Here, also the values of BLKT parameters shown in the inset plots are used in our analysis. The two left panels ((a) and (c)) show the range of BLKT parameter space which we will use in $t\bar{t}$-resonance production, whereas the two right panels ((b) and (d)) show the range of BLKT parameter space for $\ell^+\ell^-$ resonance production. In all the cases, the KK-masses are decreased with the increasing positive values of BLKTs. The detail characteristic features of these plots can be found in [36, 43, 44].

3. KK-parity-non-conserving coupling of $V^1(\equiv G^1, B^1$ and $W_3^1)$ with zero mode fermions

Conservation of KK-parity is an inherent property of UED model, even it is still conserved in the presence of BLTs of equal strength. However, non-conservation of KK-parity can be generated with unequal strength of BLTs. In our work, we originate this non-conservation in two different ways. In one set-up, we consider the strengths of BLKTs for fermions equal at the boundary points *i.e.*, $r^a_f = r^b_f \equiv r_f$, while for the gauge bosons $r^a_V \neq r^b_V$. In the other option, we assume that the BLKTs are present only at the $y = 0$ fixed point for both the fermions and the gauge bosons. Utilising the above alternatives, we give rise to the interacting coupling between gauge boson at $n = 1$ KK-level with pair of SM (zero mode) fermions, and it is given by [36, 43, 44]

$$g_{V^1 f^0 f^0} = \begin{cases} \tilde{g} \int_0^{\pi R} \mathrm{d}y \ \left[1 + r^a_f \delta(y) + r^b_f \delta(y - \pi R)\right] f^0_{\mathrm{L}} f^0_{\mathrm{L}} a^1 \,, \\ \tilde{g} \int_0^{\pi R} \mathrm{d}y \ \left[1 + r^a_f \delta(y) + r^b_f \delta(y - \pi R)\right] g^0_{\mathrm{R}} g^0_{\mathrm{R}} a^1 \,. \end{cases} \tag{14}$$

$\tilde{g}$ represents 5-D gauge coupling which is connected to the conventional 4-D gauge coupling g through the following relation [36, 43, 44]:

$$\tilde{g} = g\sqrt{\pi R\left(1 + \frac{r^a_V + r^b_V}{2\pi R}\right)}\,. \tag{15}$$

Here, $f_{\rm L}^0, g_{\rm R}^0$ are denoted as wave functions for zero mode fermion and a^1 is identified as a wave function for the first excited state ($n = 1$) of KK-gauge bosons.

In our first choice, y-dependent wave functions are given as follows:

$$f_{\rm L}^0 = g_{\rm R}^0 = \frac{1}{\sqrt{\pi R\left(1+\frac{R_f}{\pi}\right)}} \tag{16}$$

and

$$a^1 = N_1^V\left[\cos\left(\frac{M_{(1)}y}{R}\right) - \frac{R_V^a M_{(1)}}{2}\sin\left(\frac{M_{(1)}y}{R}\right)\right], \tag{17}$$

with normalisation constant

$$N_1^V = \sqrt{\frac{1}{\pi R}} \times \sqrt{\frac{8\left(4+M_{(1)}^2 R_V^{b\,2}\right)}{2\left(\frac{R_V^a+R_V^b}{\pi}\right)\left(4+M_{(1)}^2 R_V^a R_V^b\right)+\left(4+M_{(1)}^2 R_V^{a\,2}\right)\left(4+M_{(1)}^2 R_V^{b\,2}\right)}},$$

where, $M_{(1)} = m_{V^{(1)}}R$, $R_f = r_f R^{-1}$, $R_V^a = r_V^a R^{-1}$, and $R_V^b = r_V^b R^{-1}$. Utilising the above, we finally acquire the effective 4-D coupling [36, 43, 44]

$$g_{V^1 f^0 f^0} = \frac{g\sqrt{\pi R\left(1+\frac{R_V^a+R_V^b}{2\pi}\right)}N_1^V}{\left(1+\frac{R_f}{\pi}\right)}\left[\frac{\sin(\pi M_{(1)})}{\pi M_{(1)}}\left\{1-\frac{M_{(1)}^2 R_V^a R_f}{4}\right\}\right.$$
$$\left.+\frac{R_V^a}{2\pi}\left\{\cos\left(\pi M_{(1)}\right)-1\right\}+\frac{R_f}{2\pi}\left\{\cos\left(\pi M_{(1)}\right)+1\right\}\right]. \tag{18}$$

This coupling vanishes for the equality condition $R_V^a = R_V^b$ [36, 43, 44].

In the second case, the y-dependent wave functions are given by

$$f_{\rm L}^0 = g_{\rm R}^0 = \frac{1}{\sqrt{\pi R\left(1+\frac{R_f}{2\pi}\right)}} \tag{19}$$

and

$$a^1 = \sqrt{\frac{2}{\pi R}}\sqrt{\frac{1}{1+\left(\frac{R_V M_{(1)}}{2}\right)^2+\frac{R_V}{2\pi}}} \times\left[\cos\left(\frac{M_{(1)}y}{R}\right)-\frac{R_V M_{(1)}}{2}\sin\left(\frac{M_{(1)}y}{R}\right)\right]. \tag{20}$$

We obtain for this choice [36, 43, 44]

$$g_{V^1 f^0 f^0} = \frac{\sqrt{2}\, g \sqrt{\left(1+\frac{R_V}{2\pi}\right)}}{\left(1+\frac{R_f}{2\pi}\right)\sqrt{1+\left(\frac{R_V M_{(1)}}{2}\right)^2+\frac{R_V}{2\pi}}}\left(\frac{R_f-R_V}{2\pi}\right). \tag{21}$$

This coupling disappears when $R_f = R_V$ [36, 43, 44]. It can be easily checked from the lower panels of Fig. 2.

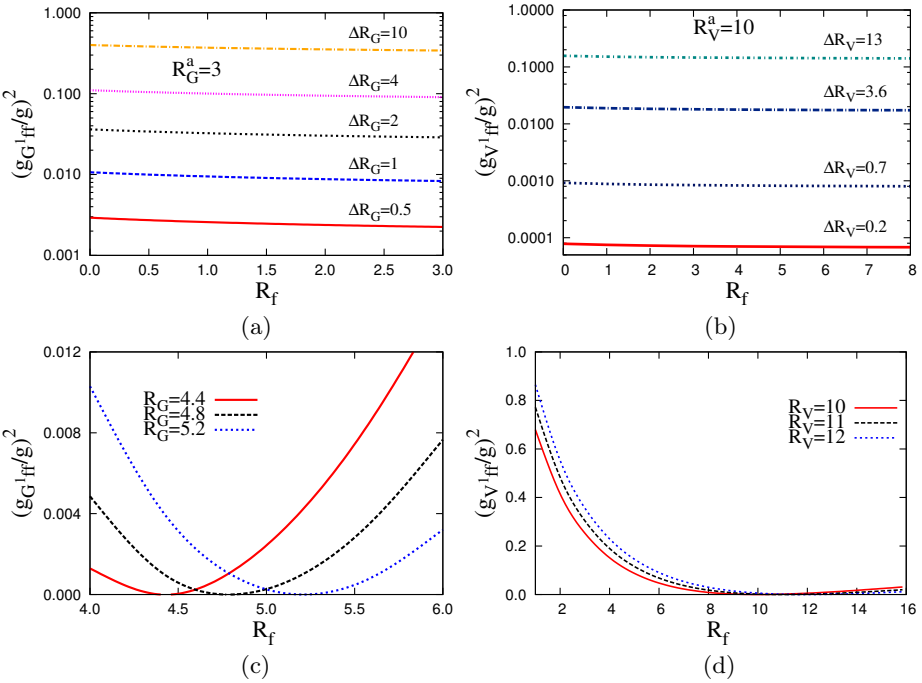

Fig. 2. The upper (a) and lower (c) panels of the left-hand side show the variation of $(g_{G^1 f^0 f^0}/g)^2$ as a function of BLKT parameters what we use in $t\bar{t}$ production. Similarly, the upper (b) and lower (d) panels of the right-hand side show the variation of $(g_{V^1 f^0 f^0}/g)^2$ corresponding to $\ell^+\ell^-$ production. For the purpose of detailed illustrations, one can see the text and also Refs. [36, 43, 44].

In Fig. 2, we have shown the variation of scaled KK-parity non-conserving coupling which can be termed as overlap integrals[6] for different cases. A care-

[6] Effective interactions in this model can be achieved by integrating out the 5-D action over the extra space-like dimension after replacing the appropriate y-dependent KK-wave-function for the respective fields in 5-D action, see Eq. (14). Consequently, some of the interactions are modified by some multiplicative factors which are called overlap integrals.

ful look at the upper panels ((a) and (b)) reveal that the KK-parity non-conserving coupling rises with increasing values of asymmetric parameter $\Delta R_\alpha = (R^b_\alpha - R^a_\alpha)$ $(\alpha \equiv G, B, W_3)$, while decreases with the increasing values of R^a_α. The magnitude of KK-parity non-conserving coupling decreases mildly with the greater values of R_f. In the lower panels ((c) and (d)), the coupling shows oscillatory nature with R_f. However, in the region of our interest $(R_V(R_G) > R_f)$, the KK-parity-non-conserving coupling rises with higher values of R_G (R_V). We have shown the values of the coupling strengths with BLKT parameters which we use in our analysis. The detailed dependence of this coupling strength with respect to the BLKT parameters can be found in Refs. [36, 43, 44].

4. Gauge boson $V^1(\equiv G^1, B^1$ and $W^1_3)$ production and decay

Up to this point we have all the required ingredients to discuss some phenomenological signals of nmUED. Specifically, at the LHC, we are interested in investigating the resonant production of $pp \to V^1$ followed by the decay $V^1 \to f^0 \bar{f}^0$, with f^0 being the SM quarks or leptons[7]. Both the production and the decay of V^1 are governed by KK-parity non-conserving couplings which vanish if the strengths of BLT parameters at two boundary points are the same [36, 43, 44]. A compact expression for the production cross section in pp collisions can be written as

$$\sigma(pp \to V^1 + X) = \frac{4\pi^2 N_c}{3m^3_{V^{(1)}}} \sum_i \Gamma(V^1 \to q_i\bar{q}_i)\tau \times \int_\tau^1 \frac{\mathrm{d}x}{x}\left[f_{\frac{q_i}{p}}\left(x, m^2_{V^{(1)}}\right) f_{\frac{\bar{q}_i}{p}}\left(\tau/x, m^2_{V^{(1)}}\right) + q_i \leftrightarrow \bar{q}_i\right]. \quad (22)$$

Here, q_i and $\bar{q}_i$ represent a generic quark and its antiquark of the i^{th} flavour respectively. Quark (antiquark) distribution function within a proton is represented by $f_{\frac{q_i}{p}}$ $(f_{\frac{\bar{q}_i}{p}})$. We denote $\tau = m^2_{V^{(1)}}/S$, where $\sqrt{S}$ is the pp centre-of-momentum energy and N_c is the colour factor. $\Gamma(V^1 \to q_i\bar{q}_i)$ is the decay width of V^1 into the SM quark–antiquark pair $(q_i\bar{q}_i)$. In the case of $pp \to G^1 \to t\bar{t}$ channel, we have not considered higher order perturbative QCD corrections in our analysis, as QCD corrections usually increase cross sections. In this regard, our results are probably conservative.

Decay width of G^1 ($n = 1$ KK-excitation of *gluon*) into $q_i\bar{q}_i$ pair is given by $\Gamma = \left[\frac{g^2_{V^1 qq}}{\pi}\right] m_{G^{(1)}}$. In the case of B^1 ($n = 1$ KK-excitation of $\mathrm{U}(1)_Y$

[7] From now and onwards, we will not use superscript "0" for SM particles.

gauge boson), one has $\Gamma = \left[\frac{g^2_{V^1qq}}{32\pi}\right] \left[(Y^q_{\rm L})^2 + (Y^q_{\rm R})^2\right] m_{B^{(1)}}$ (with $Y^q_{\rm L}$ and $Y^q_{\rm R}$ being the weak-hypercharges for the left- and right-chiral quarks), while the decay width of W^1_3 ($n = 1$ KK-excitation of neutral $\mathrm{SU}(2)_{\rm L}$ gauge boson) given by $\Gamma = \left[\frac{g^2_{V^1qq}}{32\pi}\right] m_{W^{(1)}_3}$. g_{V^1qq} represents the KK-parity non-conserving coupling between $q_i\bar{q}_i$ pair and V^1 as given in Eqs. (18) and (21). In the expression of cross section (see Eq. (22)), $m_{V^{(1)}}$ denotes the mass eigenvalue of the gauge boson of $n = 1$ KK-excitation. The KK-modes of electroweak gauge bosons (B and W_3) also acquire a contribution to their masses from spontaneous breaking of the electroweak symmetry, however that contribution is not taken into account in our analysis as they are negligible in comparison to extra dimensional contribution. Hence, B^1 and W^1_3 share the same mass eigenvalue.

To determine the numerical values of the cross sections, we use a parton level Monte Carlo code with parton distribution functions as parametrized in CTEQ6L [51]. In this analysis, the pp centre-of-momentum energy is 13 TeV. Further, we set factorisation scales (in the parton distributions) and renormalisation scale for $\alpha_{\rm s}$ at $m_{V^{(1)}}$.

We have contrasted the above outcome with two different results from the LHC. In the following sections, we are going to present the search of $t\bar{t}$ and $\ell^+\ell^-$ resonances at the LHC running at 13 TeV pp centre-of-momentum energy. We assume G^1 or $B^1(W^1_3)$ to be the lightest KK-particles (LKP) in the respective cases. In this situation, after the production of G^1 or $B^1(W^1_3)$ (first excited KK gauge boson), the KK-parity conserving decays being kinematically disallowed, the G^1 or $B^1(W^1_3)$ decays to a pair of zero-mode fermions (quarks or charged leptons) via the same KK-parity non-conserving coupling. From the lack of observation of such signals at 95% C.L., upper bounds have been established on the cross section times branching fraction[8] as a function of the mass of a $t\bar{t}$ and/or $\ell^+\ell^-$ resonance. Comparing these bounds with the theoretical predictions in the KK-parity non-conserving framework, one can constrain the parameter space of this nmUED model. To acquire the most up-to-date bounds, we use the latest 13 TeV results from the CMS [7] and ATLAS [8] data for $t\bar{t}$- and $\ell^+\ell^-$-resonance production respectively. Results for two different signals for two distinct cases, either BLKTs are non-vanishing at both boundary points or only at one of the two, will be presented in following two sections.

[8] The branching fraction of G^1 to $t\bar{t}$ is nearly $\frac{1}{6}$ and for B^1 (W^1_3) to e^+e^- and $\mu^+\mu^-$ is nearly $\frac{30}{103}$ $\left(\frac{2}{21}\right)$.

5. $t\bar{t}$-resonance search at 13 TeV and comparative study with 8 TeV analysis

In this section, we have shown the excluded region of parameter space of the nmUED model utilising $t\bar{t}$-resonance production data of accumulated luminosity 2.6 fb^{-1} reported by the CMS Collaboration [7].

Case 1: BLKTs are present at $y = 0$ and $y = \pi R$

In this case, we have considered that the BLKTs for fermions are equal at the two fixed boundary points, while KK-parity is broken by the unequal strengths of the gluon BLKTs. In Fig. 3, there are three panels corresponding to three different values of R^a_G. In a particular panel, there are several curves corresponding to different values of ΔR_G. For a specific value of R^a_G, there is one-to-one correspondence of $m_{G^{(1)}}$ with R^{-1} which is shown on the upper axis of the panels, as the KK-mass is mildly-dependent upon ΔR_G. Furthermore, one can determine $m_{f^{(1)}}$ using $M_{f^{(1)}} = m_{f^{(1)}} R$ corresponding to a particular value of R_f and is displayed on the right-hand side axis.

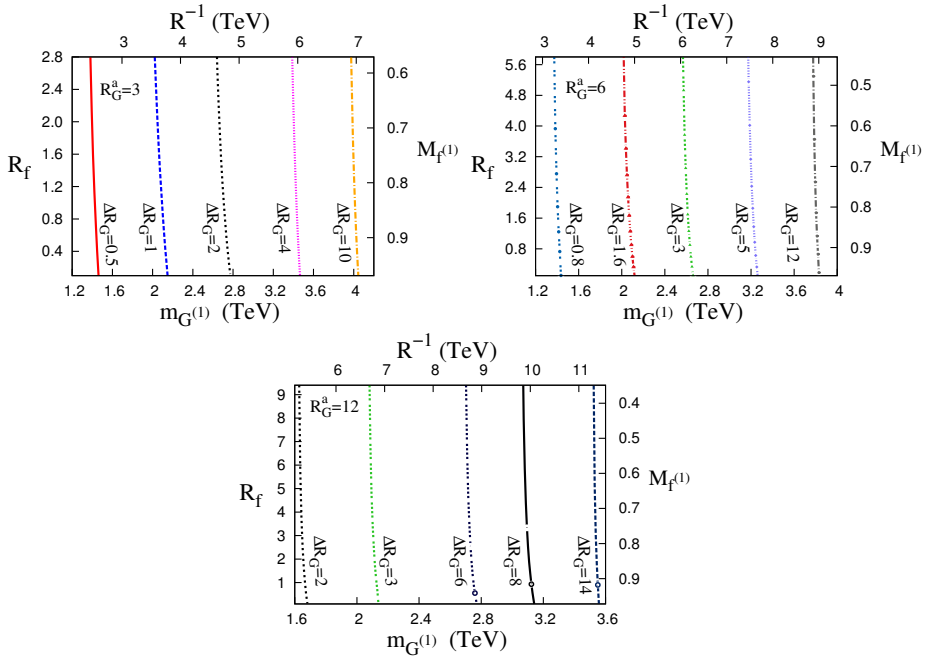

Fig. 3. Using the data of non-observation of a resonant production channel of $t\bar{t}$ signal at the LHC running at 13 TeV, we have shown excluded/allowed regions at 95% C.L. in the $m_{G^{(1)}}$–R_f plane for several choices of $\Delta R_G = (r^b_G - r^a_G)R^{-1}$. Each panel is specified by a particular value of R^a_G. The region to the left of a given curve is excluded by the CMS data [7]. R^{-1} and $M_{f^{(1)}} (= m_{f^{(1)}} R)$ are shown on the upper and right-hand side axes respectively. "G" stands for gluon.

In each panel of Fig. 3, the left portion of a curve specified by a fixed value of ΔR_G in the $m_{G^{(1)}}$–R_f plane is excluded by the CMS data [7] at 95% C.L. The exclusion plots presented in Fig. 3 can easily be understood by conjunction of the two plots given in Figs. 1 and 2. From Fig. 2 (a), it is seen that KK-parity non-conserving coupling is almost insensitive to R_f, while increases with ΔR_G. Therefore, the resonance production cross section effectively depends on R_G^a and ΔR_G. Again from Fig. 1 (a), it is clear that for a fixed value of R_G^a, the KK-mass decreases with increasing values of ΔR_G. One can check from the CMS data that the cross section also decreases with increasing resonance mass. Therefore, in order to match the observed data, we need larger values of KK-parity non-conserving coupling due to the increment of $m_{G^{(1)}}$. Hence, we need larger values of ΔR_G for a fixed values of R_f. Now, if we take a larger value of R_G^a, we need higher value of R^{-1} than that by which we obtain the same resonance mass for lower values of R_G^a. At the same time, higher values of R_G^a bring the higher values of R_f. One should note that for any fixed value of R_G^a (any one panel), the entire range of the mass given in the data cannot be covered. This happens, in order to match with the data, the KK-parity non-conserving coupling which requires for the model prediction of cross section for a particular $m_{G^{(1)}}$ varies only over a restricted range. These features are consistent with results in Fig. 3.

Now, we are in a stage where we can discuss the deviation of the limits of the model parameters by comparing the results obtained from current 13 TeV LHC analysis with the previous 8 TeV LHC analysis [43]. Before going into that, let us spend some time to discuss the behaviour of resonance production cross section at 13 TeV LHC [7]. In this case, the resonance production cross section for a particular mass is larger with respect to previous 8 TeV results [52]. One can explain this phenomena in the following way. For a resonance production, the typical x (given in Eq. (22)) values which we are probing are of the order of $\tau(\equiv m_{t\bar{t}}^2/S)$. A higher S implies lower τ, thus it not only increases the range of x integration, but also includes this region of x for which parton density functions are higher in magnitude[9].

If we translate the above phenomena in a particular panel specified by a particular value of R_G^a, then we can see that a smaller strength of KK-parity non-conserving coupling is sufficient to match the model prediction with the new 13 TeV LHC data. Now KK-parity non-conserving coupling diminishes if we decrease the values of ΔR_G which, in turn, enhance the KK-mass (in this case $t\bar{t}$-resonance mass). Thus, in this situation to obtain a specific value

[9] A similar explanation is also valid for $\ell^+\ell^-$-resonance production at the LHC which will be discussed in the next section. In this case also, for a particular resonance mass, the production cross section for the $\ell^+\ell^-$-resonance signal is larger with respect to the previous 8 TeV data [53].

of resonance mass we need smaller value of R^{-1} than that of 8 TeV analysis. For example, if we consider the $t\bar{t}$-resonance mass 1.4 TeV for $R_G^a = 3$, the values of other model parameters are $\Delta R_G = 0.5$, $R^{-1} = 2.5$ TeV and $R_f = 1.53$ (corresponding fermion mass at first KK-excitation is 1.89 TeV) for $\sqrt{S} = 13$ TeV. However, when $\sqrt{S} = 8$ TeV, in the same set of conditions, the values of $\Delta R_G = 0.6$, $R^{-1} = 2.6$ and $R_f = 1.61$ (corresponding fermion mass at first KK-excitation was 1.95 TeV) [43]. Consequently, the exclusion plots corresponding to different values of ΔR_G have been shifted towards the higher mass (resonance mass) region with respect to 8 TeV analysis. Thus, in the current article, we probe the higher mass region with smaller values of BLKT parameters (see Fig. 3). Further, the mass gap between $m_{f^{(1)}}$ and $m_{G^{(1)}}$ decreases as the value of $\sqrt{S}$ increases. This characteristics is also valid for other panels specified by different R_G^a.

Case 2: BLKTs are present only at $y = 0$

Now, let us consider the case when fermion and gluon BLKTs are non-vanishing at only one fixed boundary point ($y = 0$). In Fig. 4, we show the exclusion limits obtained by the 13 TeV results of the CMS Collaboration [7] for $t\bar{t}$-resonance search. Here, we have shown the exclusion plots in the $m_{G^{(1)}}$–R_f plane for different values of R_G. The lower portion of a curve specified by R_G has been excluded by the 13 TeV LHC data.

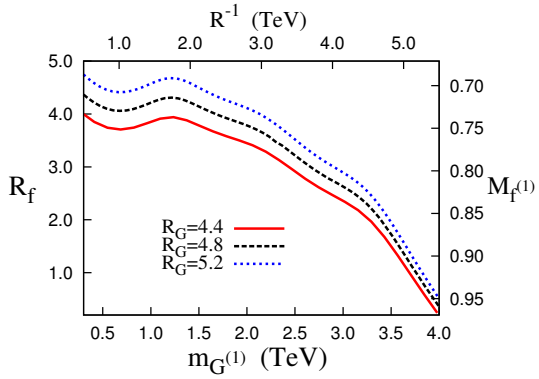

Fig. 4. Utilising the data of non-observation of a resonant $t\bar{t}$ signal at the LHC running at 13 TeV, we have shown the exclusion plots at 95% C.L. in the $m_{G^{(1)}}$–R_f plane for several choices of R_G. The region below a particular curve is ruled out from the non-observation of a resonant $t\bar{t}$ signal in the 13 TeV run of the LHC by CMS data [7]. R^{-1} and $M_{f^{(1)}} (= m_{f^{(1)}} R)$ are shown on the upper and right-hand side axes respectively. "G" stands for gluon.

We can explain the exclusion plots on the basis of bottom left panels of Figs. 1 and 2. It is quite evident from Fig. 1 (c) that $M_{(1)}(= m_{G^{(1)}}R)$ shows mild dependence on the value of R_G. So, approximately, one can take the mass of G^1 to be simply proportional to R^{-1}. The values of R^{-1} are displayed on the upper axes of the panels in Fig. 4. For any $m_{G^{(1)}}$, the CMS data provides a limit for the corresponding cross section times branching ratio. If we set the mass as fixed quantity, the experimental bound can be obtained by a specific value for the KK-parity non-conserving coupling, which is a function R_G and R_f. Alternatively, this can be viewed in the following way. As with increasing values of $m_{G^{(1)}}$ the production cross section decreases, to compensate this, the KK-parity non-conserving coupling should be increased. At this point, if we look at Fig. 2 (c), we can see that KK-parity non-conserving coupling shows oscillatory nature. However, we are interested in a region where G^1 is LKP, *i.e.*, $m_{f^{(1)}} > m_{G^{(1)}}$, which belongs to a region where $R_G > R_f$. In this region, KK-parity coupling increases with the increasing values of R_G. This is reflected in Fig. 4.

Now in this single brane set-up, we would like to point out the departure of the limits of the model parameters obtained from the current 13 TeV analysis with respect to the 8 TeV analysis [43]. We have already discussed that KK-parity non-conserving coupling of lower strength is sufficient to match the model prediction with the 13 TeV LHC data [7]. Thus in the region where $R_G > R_f$, we can obtain lower strength of KK-parity non-conserving coupling by smaller values of R_G. This can easily probe the new 13 TeV LHC data. Let us consider the value of $t\bar{t}$-resonance mass at 1 TeV, the corresponding cross sectional value can easily be matched by lower values of R_G, *e.g.*, 4.4 or 4.8. However, in the case of 8 TeV analysis, the same set of conditions demands higher values of R_G, *e.g.*, 5.0 [43]. As an artifact, the values of R_f have also been reduced in the 13 TeV analysis. For example, in the case of 13 TeV analysis, the values of R_f corresponding to the above-mentioned values of R_G are 3.84 and 4.20, respectively, while in the case of 8 TeV analysis, the value of R_f was 4.5. This result revealed that the lower limits of BLKT parameters have been reduced due to higher centre-of-momentum energy ($\sqrt{S}$).

6. $\ell^+\ell^-$-resonance search at 13 TeV and relative study with 8 TeV analysis

Exactly in the same way as in the case of the $t\bar{t}$-resonance search, we have examined another signal at the LHC using the virtue of KK-parity non-conservation. In this case, we have calculated the (resonance) production cross section of $B^1(W_3^1)$ in pp collisions at the LHC and their subsequent decay to e^+e^- and $\mu^+\mu^-$, assuming $B^1(W_3^1)$ to be the lightest KK-particles.

We can exclude some portion of parameter space of this nmUED model using the 13 TeV LHC data of integrated luminosity 36.1 fb^{-1} of the ATLAS Collaboration [8] for $\ell^+\ell^-(\ell \equiv e, \mu)$-resonance production.

Case 1: BLKTs are present at $y = 0$ and $y = \pi R$

Figure 5 represents the case when the strengths of BLKTs for fermions are equal at both the boundary points, however, the strengths of BLKTs for electroweak gauge boson are unequal. Here, we have shown the region excluded by the 13 TeV LHC data [8] in two panels specified by different values of R_V^a. In the $m_{V^{(1)}}$–R plane, the left region of a given curve specified by ΔR_V has been excluded by the LHC data [8]. For any displayed value of R_f, we can measure the corresponding mass for the first KK-excitation of fermion using $M_{f^{(1)}} = m_{f^{(1)}} R$ (plotted on right-side axis). The relevant values of R^{-1} have been plotted on upper-side axis.

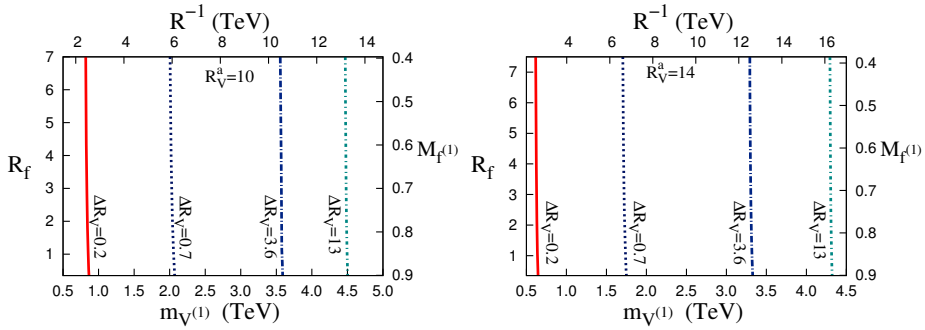

Fig. 5. Using the non-observation of a resonant $\ell^+\ell^-$ signal at the LHC running at 13 TeV, we have shown excluded/allowed regions at 95% C.L. in the $m_{V^{(1)}}$–R_f plane for different choices of $\Delta R_V = (r_V^b - r_V^a)R^{-1}$. Each panel is specified by a particular value of R_V^a. The region to the left of a given curve is excluded by the ATLAS data [8]. R^{-1} and $M_{f^{(1)}} (= m_{f^{(1)}} R)$ are shown on the upper and right-hand side axes respectively. "V" stands for B/W_3.

As we have already mentioned, for a chosen value of ΔR_V and R_V^a, the KK-parity non-conserving couplings are almost independent of R_f. Thus, R_f has no governance on the production of $e^+e^-/\mu^+\mu^-$. Consequently, signal rate is almost driven by R_V^a and ΔR_V. Furthermore, nature of the exclusion plots is very similar to the case of $t\bar{t}$-resonance signal. Therefore, following the same explanations (given for Fig. 3) for $t\bar{t}$ signal, one can easily understand the exclusion plots of $\ell^+\ell^-$-resonance signal with the help of Fig. 1 (b) and Fig. 2 (b).

Despite the similar behaviour of the exclusion plots of the two different signals (for double brane set-up) at the LHC, a unique feature has been observed in the exclusion plots (Fig. 5) for $\ell^+\ell^-$-resonance signal. In this case, the model prediction has been able to cover the entire LHC data of our concern. The reason is that the KK-parity non-conserving coupling needed for model prediction of cross section for a particular $m_{V^{(1)}}$ match with the data varies over the entire range.

Let us see the deviations of the limits of the model parameters achieved from the 13 TeV analysis with that obtained from 8 TeV analysis [44]. To match the model prediction with the new 13 TeV LHC data [8], we require lower strength of KK-parity non-conserving coupling. One can achieve this by reducing the value of ΔR_V. However, it enhances the KK-mass (in this case $\ell^+\ell^-$-resonance mass). Therefore, to generate a typical value of resonance mass, we need lower value of R^{-1} than that of thee 8 TeV analysis. For example, if we choose the $\ell^+\ell^-$-resonance mass as 2 TeV for $R_V^a = 10$, the values of $\Delta R_V = 0.7$, $R^{-1} = 5.9$ TeV and $R_f = 6.64$. The corresponding fermion mass at first KK-excitation is 2.50 TeV. However, in the case of 8 TeV analysis, under the same set of conditions, the values were $\Delta R_V = 1.5$, $R^{-1} = 7.9$ and $R_f = 6.70$ (corresponding fermion mass at first KK-excitation was 3.32 TeV) [44]. Hence, in the case of 13 TeV analysis, the exclusion curves specified by different values of ΔR_V have been shifted towards the higher mass (resonance mass) region with respect to the 8 TeV analysis. Therefore, analysis with higher centre-of-momentum energy probe the higher mass region with relatively lower values of BLKT parameters (see Fig. 5). In this case, also the mass gap between $m_{f^{(1)}}$ and $m_{V^{(1)}}$ diminishes with increasing values of $\sqrt{S}$.

Case 2: BLKTs are present only at $y = 0$

Let us study the case when fermion and electroweak gauge boson BLKTs are present at only one special boundary point ($y = 0$). In Fig. 6, we have plotted the exclusion curves in the $m_{V^{(1)}}$–R_f plane for different choices of R_V. The lower portion of a curve has been disfavoured by the 13 TeV LHC data [8].

In this case, one can also see that the exclusion plots presented in Fig. 6 show the same behaviour as in the respective case of $t\bar{t}$ signal. Therefore, on the basis of Fig. 1 (d) and Fig. 2 (d), it would not be difficult to understand the exclusion plots given in Fig. 6. It is quite evident from Fig. 1 (d) that $M_{(1)} (= m_{V^{(1)}} R)$ has mild dependence on R_V. One can thus take the mass of $V^1 (\equiv B^1, W_3^1)$ to be nearly proportional to R^{-1} (the relevant values of R^{-1} are displayed in the upper axis of Fig. 6). Here, we can also find the KK-fermion mass of first excitation in a correlated way (using $M_{f^{(1)}} = m_{f^{(1)}} R$) from the right-hand side axis of this plot.

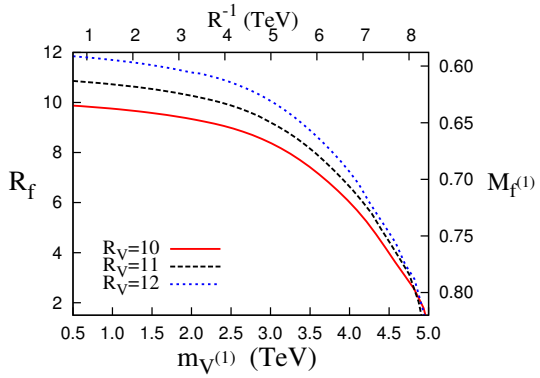

Fig. 6. Utilising the non-observation of a resonant $\ell^+\ell^-$ signal at the LHC running at 13 TeV, we have shown the exclusion plots at 95% C.L. in the $m_{V^{(1)}}$–R_f plane for several choices of R_V. The region below a particular curve is ruled out from the non-observation of a resonant $\ell^+\ell^-$ signal in the 13 TeV run of LHC by ATLAS data [8]. R^{-1} and $M_{f^{(1)}} (= m_{f^{(1)}} R)$ are shown in the upper and right-hand side axes respectively. "V" stands for B/W_3.

Now, we are going to discuss the difference between the limits of the model parameters obtained from the current 13 TeV analysis and the 8 TeV analysis [44]. We are particularly interested in a region where V^1 is LKP, for which we require $R_V > R_f$. If we see Fig. 2 (d) then it will be understood that the region where $R_V > R_f$, the driving KK-parity non-conserving coupling decreases with the increasing values of R_f. As the 13 TeV analysis demands lower strength of KK-parity non-conserving coupling to match the experimental data, one can achieve the lower strength of KK-parity non-conserving coupling by increasing the values of R_f. This is exactly reflected in the current analysis. For example, we set the $\ell^+\ell^-$-resonance mass at 1.5 TeV and set the value of R_V at 11. The corresponding value of R_f is 10.537 for which the value of fermion mass $(m_{f^{(1)}})$ of first KK-excitation is 1.5024 TeV. For the 8 TeV analysis in the same set of conditions, the value of R_f was 10.239 and the corresponding value of $m_{f^{(1)}}$ was 1.5072 [44]. This result provide the information that if we increase the value of centre-of-momentum energy, the value of R_f increases which, in turn, decreases the mass gap between $m_{f^{(1)}}$ and $m_{V^{(1)}}$.

7. Conclusions

We have studied the phenomenology of KK-parity non-conserving UED model where all the SM fields are allowed to propagate in (4+1)-dimensional space-time. We have produced the non-conservation of KK-parity by adding boundary localised terms of unequal strengths at the two boundary points of

S^1/Z_2 orbifold. These boundary localised terms can be identified as cutoff-dependent log divergent radiative corrections which play a crucial role to remove mass degeneracy in the KK-mass spectrum of the effective (3+1)-dimensional theory.

In this paradigm, we have produced KK-parity non-conservation in two different ways. In the first case, we choose equal strengths of boundary terms for fermions at the two fixed boundary points ($y = 0$ and $y = \pi R$) and parametrised by r_f, while we have considered unequal strengths of boundary terms ($r_V^a \neq r_V^b$) for gauge boson. In the other set-up, we have considered non-vanishing boundary terms for fermion and gauge boson only at the fixed point $y = 0$. The driving KK-parity non-conserving coupling vanishes in the $\Delta R_V = 0$ limit in the first case, and for $R_f = R_V$, in the later case. In these set-ups, we calculate *two different* types of signal rate at the 13 TeV LHC. Specifically, production of first KK-excitation of gluon (G^1) and its decay to $t\bar{t}$ pair. In the other case, we study the production of first KK-excitation of neutral electroweak gauge bosons (B^1 and W_3^1) and their decay to e^+e^- and $\mu^+\mu^-$ pair. Both the production and decay are the direct consequences of KK-parity non-conservation. We compare our model predictions with the $t\bar{t}$- and $\ell^+\ell^-(\ell \equiv e, \mu)$-resonance production rate at the LHC running at 13 TeV pp centre-of-momentum energy. The lack of observation of these signals at the LHC excludes a finite portion of the parameter space of this model.

Furthermore, in this article, we have compared the limits obtained from the current 13 TeV analysis with that of previous 8 TeV analysis. With the increasing value of centre-of-momentum energy, the parton density function with higher amplitude is folded in the production cross section. Hence, relatively lower strength of KK-parity non-conserving coupling is adequate to match the model prediction with the experimental data. However, in the case of 8 TeV analysis, the required strength of KK-parity non-conserving coupling was higher with respect to present situation. Thus, the change in relative strength of KK-parity non-conserving coupling has far reaching consequences in the model parameters. In both scenarios for both signals, the values of parameters have been significantly changed. In the case of double brane set-up, for both the signals, the asymmetric parameter (ΔR_V) is shifted towards the lower values, which immediately pushed the values of R^{-1} towards the lower side. Apart from this, the limits of fermionic BLT parameter (R_f) also decrease with that of the 8 TeV analysis. Therefore, the mass gap between the resonance mass and the mass of first KK-excitation of the corresponding fermions has been diminished. In the case of single brane set-up, the 13 TeV analysis of $t\bar{t}$-resonance production decreases the values of R_G with respect to the 8 TeV analysis. However, the $\ell^+\ell^-$-resonance production increases the values of R_f compare to the 8 TeV analysis.

The author thanks Anindya Datta for many useful discussions.

REFERENCES

[1] G. Aad *et al.* [ATLAS Collaboration], *Phys. Lett. B* **716**, 1 (2012) [arXiv:1207.7214 [hep-ex]].

[2] S. Chatrchyan *et al.* [CMS Collaboration], *Phys. Lett. B* **716**, 30 (2012) [arXiv:1207.7235 [hep-ex]].

[3] G. Aad *et al.* [ATLAS Collaboration], *J. High Energy Phys.* **1512**, 55 (2015) [arXiv:1506.00962 [hep-ex]].

[4] V. Khachatryan *et al.* [CMS Collaboration], *Eur. Phys. J. C* **74**, 3149 (2014).

[5] B. Bhattacherjee *et al.*, *Phys. Rev. D* **88**, 035011 (2013).

[6] B. Bhattacherjee *et al.*, *Phys. Rev. D* **93**, 075004 (2016).

[7] A.M. Sirunyan *et al.* [CMS Collaboration], *J. High Energy Phys.* **1707**, 001 (2017) [arXiv:1704.03366 [hep-ex]].

[8] M. Aaboud *et al.* [ATLAS Collaboration], *J. High Energy Phys.* **1710**, 182 (2017) [arXiv:1707.02424 [hep-ex]].

[9] T. Appelquist, H.C. Cheng, B.A. Dobrescu, *Phys. Rev. D* **64**, 035002 (2001) [arXiv:hep-ph/0012100].

[10] P. Nath, M. Yamaguchi, *Phys. Rev. D* **60**, 116006 (1999) [arXiv:hep-ph/9903298].

[11] I. Antoniadis, *Phys. Lett. B* **246**, 377 (1990).

[12] P. Dey, G. Bhattacharyya, *Phys. Rev. D* **69**, 076009 (2004) [arXiv:hep-ph/0309110]; *Phys. Rev. D* **70**, 116012 (2004) [arXiv:hep-ph/0407314].

[13] D. Chakraverty, K. Huitu, A. Kundu, *Phys. Lett. B* **558**, 173 (2003) [arXiv:hep-ph/0212047].

[14] A.J. Buras, M. Spranger, A. Weiler, *Nucl. Phys. B* **660**, 225 (2003) [arXiv:hep-ph/0212143]; A.J. Buras, A. Poschenrieder, M. Spranger, A. Weiler, *Nucl. Phys. B* **678**, 455 (2004) [arXiv:hep-ph/0306158].

[15] K. Agashe, N.G. Deshpande, G.H. Wu, *Phys. Lett. B* **514**, 309 (2001) [arXiv:hep-ph/0105084]; U. Haisch, A. Weiler, *Phys. Rev. D* **76**, 034014 (2007) [arXiv:hep-ph/0703064].

[16] J.F. Oliver, J. Papavassiliou, A. Santamaria, *Phys. Rev. D* **67**, 056002 (2003) [arXiv:hep-ph/0212391].

[17] T. Appelquist, H.U. Yee, *Phys. Rev. D* **67**, 055002 (2003) [arXiv:hep-ph/0211023]; G. Belanger *et al.*, *EPJ Web Conf.* **28**, 12070 (2012) [arXiv:1201.5582 [hep-ph]].

[18] T.G. Rizzo, J.D. Wells, *Phys. Rev. D* **61**, 016007 (2000) [arXiv:hep-ph/9906234]; A. Strumia, *Phys. Lett. B* **466**, 107 (1999) [arXiv:hep-ph/9906266]; C.D. Carone, *Phys. Rev. D* **61**, 015008 (2000) [arXiv:hep-ph/9907362].

[19] I. Gogoladze, C. Macesanu, *Phys. Rev. D* **74**, 093012 (2006) [arXiv:hep-ph/0605207].

[20] G. Servant, T.M.P. Tait, *New J. Phys.* **4**, 99 (2002) [arXiv:hep-ph/0209262]; *Nucl. Phys. B* **650**, 391 (2003) [arXiv:hep-ph/0206071]; H.C. Cheng, J.L. Feng, K.T. Matchev, *Phys. Rev. Lett.* **89**, 211301 (2002) [arXiv:hep-ph/0207125]; D. Majumdar, *Phys. Rev. D* **67**, 095010 (2003) [arXiv:hep-ph/0209277]; F. Burnell, G.D. Kribs, *Phys. Rev. D* **73**, 015001 (2006) [arXiv:hep-ph/0509118]; K. Kong, K.T. Matchev, *J. High Energy Phys.* **0601**, 038 (2006) [arXiv:hep-ph/0509119]; M. Kakizaki, S. Matsumoto, M. Senami, *Phys. Rev. D* **74**, 023504 (2006) [arXiv:hep-ph/0605280].

[21] G. Belanger, M. Kakizaki, A. Pukhov, *J. Cosmol. Astropart. Phys.* **1102**, 009 (2011) [arXiv:1012.2577 [hep-ph]].

[22] K.R. Dienes, E. Dudas, T. Gherghetta, *Phys. Lett. B* **436**, 55 (1998) [arXiv:hep-ph/9803466]; *Nucl. Phys. B* **537**, 47 (1999) [arXiv:hep-ph/9806292]; G. Bhattacharyya, A. Datta, S.K. Majee, A. Raychaudhuri, *Nucl. Phys. B* **760**, 117 (2007) [arXiv:hep-ph/0608208].

[23] K. Hsieh, R.N. Mohapatra, S. Nasri, *Phys. Rev. D* **74**, 066004 (2006) [arXiv:hep-ph/0604154]; Y. Fujimoto, K. Nishiwaki, M. Sakamoto, R. Takahashi, *J. High Energy Phys.* **1410**, 191 (2014) [arXiv:1405.5872 [hep-ph]].

[24] A. Datta, S. Raychaudhuri, *Phys. Rev. D* **87**, 035018 (2013) [arXiv:1207.0476 [hep-ph]]; T. Kakuda, K. Nishiwaki, K.-y. Oda, R. Watanabe, *Phys. Rev. D* **88**, 035007 (2013) [arXiv:1305.1686 [hep-ph]]; arXiv:1305.1874 [hep-ph]; G. Bélanger *et al.*, *Phys. Rev. D* **87**, 016008 (2013) [arXiv:1207.0798 [hep-ph]]; A. Belyaev, M. Brown, J.M. Moreno, C. Papineau, *J. High Energy Phys.* **1306**, 080 (2013) [arXiv:1212.4858 [hep-ph]].

[25] G. Bhattacharyya, P. Dey, A. Kundu, A. Raychaudhuri, *Phys. Lett. B* **628**, 141 (2005) [arXiv:hep-ph/0502031]; B. Bhattacherjee, A. Kundu, *Phys. Lett. B* **627**, 137 (2005) [arXiv:hep-ph/0508170]; A. Datta, S.K. Rai, *Int. J. Mod. Phys. A* **23**, 519 (2008) [arXiv:hep-ph/0509277]; B. Bhattacherjee, A. Kundu, S.K. Rai, S. Raychaudhuri, *Phys. Rev. D* **78**, 115005 (2008) [arXiv:0805.3619 [hep-ph]]; B. Bhattacherjee, *Phys. Rev. D* **79**, 016006 (2009) [arXiv:0810.4441 [hep-ph]].

[26] L. Edelhauser, T. Flacke, M. Krëmer, *J. High Energy Phys.* **1308**, 091 (2013) [arXiv:1302.6076 [hep-ph]].

[27] H. Georgi, A.K. Grant, G. Hailu, *Phys. Lett. B* **506**, 207 (2001) [arXiv:hep-ph/0012379].

[28] H.C. Cheng, K.T. Matchev, M. Schmaltz, *Phys. Rev. D* **66**, 036005 (2002) [arXiv:hep-ph/0204342].

[29] H.C. Cheng, K.T. Matchev, M. Schmaltz, *Phys. Rev. D* **66**, 056006 (2002) [arXiv:hep-ph/0205314].

[30] G.R. Dvali, G. Gabadadze, M. Kolanovic, F. Nitti, *Phys. Rev. D* **64**, 084004 (2001) [arXiv:hep-ph/0102216].

[31] M.S. Carena, T.M.P. Tait, C.E.M. Wagner, *Acta Phys. Pol. B* **33**, 2355 (2002) [arXiv:hep-ph/0207056].

[32] F. del Aguila, M. Pérez-Victoria, J. Santiago, *J. High Energy Phys.* **0302**, 051 (2003) [arXiv:hep-th/0302023]; arXiv:hep-ph/0305119.

[33] F. del Aguila, M. Pérez-Victoria, J. Santiago, *Acta Phys. Pol. B* **34**, 5511 (2003) [arXiv:hep-ph/0310353].

[34] C. Schwinn, *Phys. Rev. D* **69**, 116005 (2004) [arXiv:hep-ph/0402118].

[35] T. Flacke, A. Menon, D.J. Phalen, *Phys. Rev. D* **79**, 056009 (2009) [arXiv:0811.1598 [hep-ph]].

[36] A. Datta, U.K. Dey, A. Shaw, A. Raychaudhuri, *Phys. Rev. D* **87**, 076002 (2013) [arXiv:1205.4334 [hep-ph]].

[37] T. Flacke, K. Kong, S.C. Park, *Phys. Lett. B* **728**, 262 (2014) [arXiv:1309.7077 [hep-ph]].

[38] A. Datta, A. Shaw, *Phys. Rev. D* **93**, 055048 (2016) [arXiv:1506.08024 [hep-ph]].

[39] J. Bonnevier, H. Melbéus, A. Merle, T. Ohlsson, *Phys. Rev. D* **85**, 043524 (2012) [arXiv:1104.1430 [hep-ph]].

[40] A. Datta, U.K. Dey, A. Raychaudhuri, A. Shaw, *Phys. Rev. D* **88**, 016011 (2013) [arXiv:1305.4507 [hep-ph]].

[41] U.K. Dey, T.S. Roy, *Phys. Rev. D* **88**, 056016 (2013) [arXiv:1305.1016 [hep-ph]].

[42] A. Datta, K. Nishiwaki, S. Niyogi, *J. High Energy Phys.* **1211**, 154 (2012) [arXiv:1206.3987 [hep-ph]]; **1401**, 104 (2014) [arXiv:1310.6994 [hep-ph]].

[43] A. Datta, A. Raychaudhuri, A. Shaw, *Phys. Lett. B* **730**, 42 (2014) [arXiv:1310.2021 [hep-ph]].

[44] A. Shaw, *Eur. Phys. J. C* **75**, 33 (2015) [arXiv:1405.3139 [hep-ph]].

[45] T. Jha, A. Datta, *J. High Energy Phys.* **1503**, 012 (2015) [arXiv:1410.5098 [hep-ph]].

[46] A. Datta, A. Shaw, *Phys. Rev. D* **95**, 015033 (2017) [arXiv:1610.09924 [hep-ph]].

[47] U.K. Dey, T. Jha, *Phys. Rev. D* **94**, 056011 (2016) [arXiv:1602.03286 [hep-ph]].

[48] A. Biswas, S.K. Patra, A. Shaw, *Phys. Rev. D* **97**, 035019 (2018) [arXiv:1708.08938 [hep-ph]].

[49] T. Jha, arXiv:1604.02481 [hep-ph].

[50] A. Datta, A. Shaw, *Mod. Phys. Lett. A* **31**, 1650181 (2016) [arXiv:1408.0635 [hep-ph]].

[51] J. Pumplin *et al.*, *J. High Energy Phys.* **0207**, 012 (2002).

[52] CMS Collaboration, *Phys. Rev. Lett.* **111**, 211804 (2013) [arXiv:1309.2030 [hep-ex]].

[53] ATLAS Collaboration, ATLAS-CONF-2013-017.